

A single dual-mode gas sensor for early safety warning of Li-ion batteries: Micro-scale Li dendrite and electrolyte leakage

Wenjun Yan(闫文君), Zhishen Jin(金志燊), Zhengyang Lin(林政扬), Shiyu Zhou(周诗瑜), Yonghai Du(杜永海), Yulong Chen(陈宇龙), and Houpan Zhou(周后盘)

Citation: Chin. Phys. B, 2022, 31 (**11**): 110704. DOI: 10.1088/1674-1056/ac98a3

What follows is a list of articles you may be interested in

An all-optical phase detector by amplitude modulation of the local field in a Rydberg atom-based mixer

Xiu-Bin Liu(刘修彬), Feng-Dong Jia(贾凤东), Huai-Yu Zhang(张怀宇), Jiong Mei(梅炅), Wei-Chen Liang(梁玮宸), Fei Zhou(周飞), Yong-Hong Yu(俞永宏), Ya Liu(刘娅), Jian Zhang(张剑), Feng Xie(谢锋), and Zhi-Ping Zhong(钟志萍)

Chin. Phys. B, 2022, 31 (**9**): 090703. DOI: 10.1088/1674-1056/ac6dbb

Optoelectronic oscillator-based interrogation system for Michelson interferometric sensors

Ling Liu(刘玲), Xiaoyan Wu(吴小龑), Guodong Liu(刘国栋), Tigang Ning(宁提纲),Jian Xu(许建), and Haidong You(油海东)

Chin. Phys. B, 2022, 31 (**9**): 090702. DOI: 10.1088/1674-1056/ac4f59

Numerical study of a highly sensitive surface plasmon resonance sensor based on circular-lattice holey fiber

Jian-Fei Liao(廖健飞), Dao-Ming Lu(卢道明), Li-Jun Chen(陈丽军), and Tian-Ye Huang(黄田野)

Chin. Phys. B, 2022, 31 (**6**): 060701. DOI: 10.1088/1674-1056/ac43a5

A stopping layer concept to improve the spatial resolution of gas-electron-multiplier neutron detector

Jianjin Zhou(周建晋), Jianrong Zhou(周健荣), Xiaojuan Zhou(周晓娟), Lin Zhu(朱林), Jianqing Yang(杨建清), Guian Yang(杨桂安), Yi Zhang(张毅), Baowei Ding(丁宝卫), Bitao Hu(胡碧涛), Zhijia Sun(孙志嘉), Limin Duan(段利敏), and Yuanbo Chen(陈元柏)

Chin. Phys. B, 2022, 31 (**5**): 050702. DOI: 10.1088/1674-1056/ac398e

Finite element simulation of Love wave sensor for the detection of volatile organic gases

Yan Wang(王艳), Su-Peng Liang(梁苏鹏), Shu-Lin Shang(商树林),Yong-Bing Xiao(肖勇兵), and Yu-Xin Yuan(袁宇鑫)

Chin. Phys. B, 2022, 31 (**3**): 030701. DOI: 10.1088/1674-1056/ac3ec9

A single dual-mode gas sensor for early safety warning of Li-ion batteries: Micro-scale Li dendrite and electrolyte leakage

Wenjun Yan(闫文君)[1,2,†], Zhishen Jin(金志燊)[1], Zhengyang Lin(林政扬)[1], Shiyu Zhou(周诗瑜)[2], Yonghai Du(杜永海)[1], Yulong Chen(陈宇龙)[3,‡], and Houpan Zhou(周后盘)[1]

[1] *School of Automation, Hangzhou Dianzi University, Hangzhou* 310018, *China*

[2] *Provincial Key Laboratory of Advanced Chemical Engineering Manufacture Technology, College of Chemical and Biological Engineering, Zhejiang University, Hangzhou* 310027, *China*

[3] *Institute of Microelectronics, University of Macau, Avenida da Universidade, Taipa, Macau, China*

(Received 17 August 2022; revised manuscript received 29 September 2022; accepted manuscript online 10 October 2022)

Li dendrites and electrolyte leakage are common causes of Li-ion battery failure. H_2, generated by Li dendrites, and electrolyte vapors have been regarded as gas markers of the early safety warning of Li-ion batteries. SnO_2-based gas sensors, widely used for a variety of applications, are promising for the early safety detection of Li-ion batteries, which are necessary and urgently required for the development of Li-ion battery systems. However, the traditional SnO_2 sensor, with a single signal, cannot demonstrate intelligent multi-gas recognition. Here, a single dual-mode (direct and alternating current modes) SnO_2 sensor demonstrates clear discrimination of electrolyte vapors and H_2, released in different states of Li-ion batteries, together with principal component analysis (PCA) analysis. This work provides insight into the intelligent technology of single gas sensors.

Keywords: gas sensors, single dual-mode, multivariable sensors, Li-batteries, early safety warning

PACS: 07.07.Df, 85.30.–z, 84.37.+q, 89.60.Ec **DOI:** 10.1088/1674-1056/ac98a3

1. Introduction

To alleviate ever-growing energy consumption, electrochemical energy storage technology has been a topic of wide concern in recent years.[1,2] In particular, lithium (Li)-ion batteries (LIBs) have dominated both electronics and automotive applications due to their high energy density and reduced cost.[1,2] Unfortunately, LIB safety issues have emerged due to the flammable organic electrolytes and the intrinsic thermal properties during charge and discharge, which could result in explosion and casualties.[3–6] For the development of large-scale LIB energy storage equipment, effective safety warnings, as early as possible, are necessary and urgently required.

The current battery management system (BMS) is regarded as a crucial LIB protection system, which can detect the voltage, state of charge (SOC), and external surface temperature of the battery cell. However, the BMS is unable to detect LIB safety issues in the early stages.[1,4] For example, the external voltage of a leaking battery could be kept at almost the same level as that of a pristine battery for several hours.[4] As reported, special gas detection of LIBs could detect LIB safety issues at an earlier stage.[1,4] In particular, H_2, generated by the reaction of Li dendrites with a polymer binder, could be captured first, and over 10 min earlier than smoke and fire, in cases of LIB failure.[1] Furthermore, LIB failure is often associated with electrolyte leakage.[6,7] The main components of the LIBs' electrolyte are volatile and redox neutral solvents, such as dimethyl carbonate (DMC), diethyl carbonate (DEC), ethyl methyl carbonate (EMC) and propylene carbonate (PC).[4,8]

As is well known, semiconductor sensors have been widely used for various hazardous and flammable gases in the internet of things (IoT) due to their high sensitivity, simple mechanism and real-time response.[9,10] However, selectivity has always been the bottleneck of semiconductor gas sensors, and further limits the recognizability and intelligentization of individual sensors. Combining sensors into arrays is a common method used to mitigate the poor selectivity of sensors, with up to thousands of individual sensors.[11] Obviously, sensor arrays cannot fulfill the convenience of sensors well.

Recently, new multivariable gas sensors have been reported.[12,13] These multivariable sensors involve a sensing material and a multivariable transducer, to provide diverse and independent responses to different gases and to provide multi-gas recognition and rejection of interferences.[14,15] The measurable response signals of chemi-electrical sensors include current, capacitance, and resistance/impedance. In contrast to the single signal of DC resistive sensors, AC impedance sensors can provide a multidimensional response over a fitted frequency range, which results from the further extraction of parameters, including the dielectric constant, charge transfer resistance, double-layer capacitance and diffusion constant, and are attracting increasing attention.[6,16–18] AC sensors are

†Corresponding author. E-mail: yanwenjun@hdu.edu.cn
‡Corresponding author. E-mail: yulongchen@um.edu.mo

© 2022 Chinese Physical Society and IOP Publishing Ltd

characterized not only by low cost and a simple device configuration, but also by different frequencies producing various signals.[6]

Herein, we use DC–AC dual mode to detect organic electrolytes and H_2 possibly venting from the failed LIBs, taking a SnO_2-based sensor as an example. Multi-sensing parameters extracted from the DC current, as well as AC impedance, and the corresponding phase angle, dissipation factor and frequency data, are comprehensively analyzed. According to the principal component analysis (PCA) of multi-sensing parameters, clear discrimination of electrolyte vapors (DEC, DMC, and PC) and H_2 is proved, which could improve the accuracy and reliability of the LIBs' early safety warning system.

2. Experimental details

2.1. Material preparation and characterization

The SnO_2-based sensing material here was prepared by following Ref. [19]. Typically, 500 g of as-received SnO_2 micro-powder (2–5 μm in diameter, Jinxin Advanced Materials, China) was mixed with 1425 g deionized water under magnetic stirring, followed by addition of 75 g triethanolamine (Usolf Chemical, China) as a dispersant. Stirring and dispersion continued for 10 mins. Next, the mixture was ball-milled (WG-1L, Vgreen Nanometer Technology, China) for 2 h with balls 300 μm in diameter to produce a uniform dispersion. Finally, 1 g of tetraamminepalladium nitrate ($H_{12}N_6O_6Pd$, Aladdin, China) was added to 12 g of the as-obtained dispersion. Consequently, the acquired stable nano-dispersion, with a solid content of 15%, was the Pd-dopped SnO_2 material utilized for this work.

The morphologies of the as-prepared material were characterized using scanning electron microscopy (SEM, FEI Nanosem 430). Powder x-ray diffraction (XRD) analyses were performed on a Bruker D8 Advance diffractometer with Cu $K\alpha$ radiation ($\lambda \approx 1.54$ Å).

2.2. Gas sensing experiment design

A schematic of the bare sensor device with a pair of interdigital electrodes (IDEs) integrating a microheater is shown in Fig. S1a (supporting information). The microheater was fabricated based on silicon micro-electromechanical system (MEMS) technology, reported in our previous work.[20] The fabrication details are also described in the supporting information. The typical relationship of the heating temperature vs. the applied voltage of the microheater is shown in Fig. S1b. The complete sensor device was fabricated by facile drop-coating. Afterwards, the device was heated and maintained at 300 °C for 7 days to promote SnO_2 deposition and device aging to obtain reliable testing data.

The gas sensing tests were performed using a homemade system with an 8-L test chamber, as reported in our previous work.[21] For the analyte sensing test, a fitting concentration of the analyte (standard H_2 gas of 10×10^{-6} mol/mol, and DMC, DEC and PC vapor) was injected into the chamber. All the sensing tests were taken at ambient temperature of about 25 °C and 40% relative humidity, adjusted by an air conditioner and a humidifier. The heating temperature of the microheater was precisely controlled using a bias voltage applied by a Keithley 2602B source-meter. The sensor DC and AC signals were collected by a Keithley 2602B source-meter and a Keysight 1732C LCR meter, respectively. Principal component analysis (PCA) was calculated using the inbuilt library function of Python.

3. Results and discussion

3.1. Material analysis

The SEM image in Fig. 1(a) shows the homogeneity of the as-prepared SnO_2 powder. The XRD pattern of the as-prepared SnO_2 is shown in Fig. 1(b). Due to the tiny Pd additive, no obvious Pd peaks are detected. All the peaks are assigned to SnO_2 of tetragonal rutile (JCPDS No. 41-1445). The obvious peaks at $2\theta = 26.7°$, 33.9°, and 38° correspond to the (110), (101), and (200) planes of SnO_2, respectively. Furthermore, the SnO_2 grain size is ∼ 30–40 nm, calculated according to the XRD data.

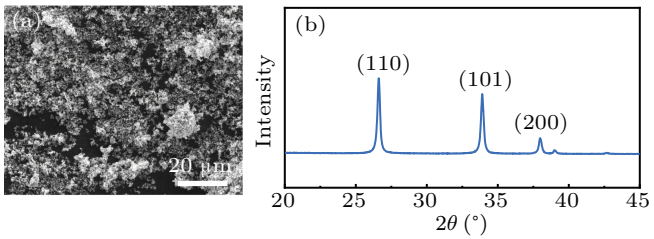


Fig. 1. (a) An SEM image, and (b) the XRD pattern of the as-prepared SnO_2 powder.

3.2. Gas sensing characteristics

We chose DEC, DMC, PC and H_2 as analyte gases, which are mainly produced by failed Li batteries. And the gas sensing performances were investigated via the DC current signal, AC impedance, θ and D signals at different frequencies. A similar AC signal response of an IDE sensor device has been reported in our previous work.[22] Figure 2 shows the relative DC and AC signal variations of one sensor device to various analyte concentrations (200, 160, 120, 80, 40, and 20 ppm of DEC, DMC, and PC, respectively; 200, 150, 100, 50, 10, and 5 ppm of H_2).

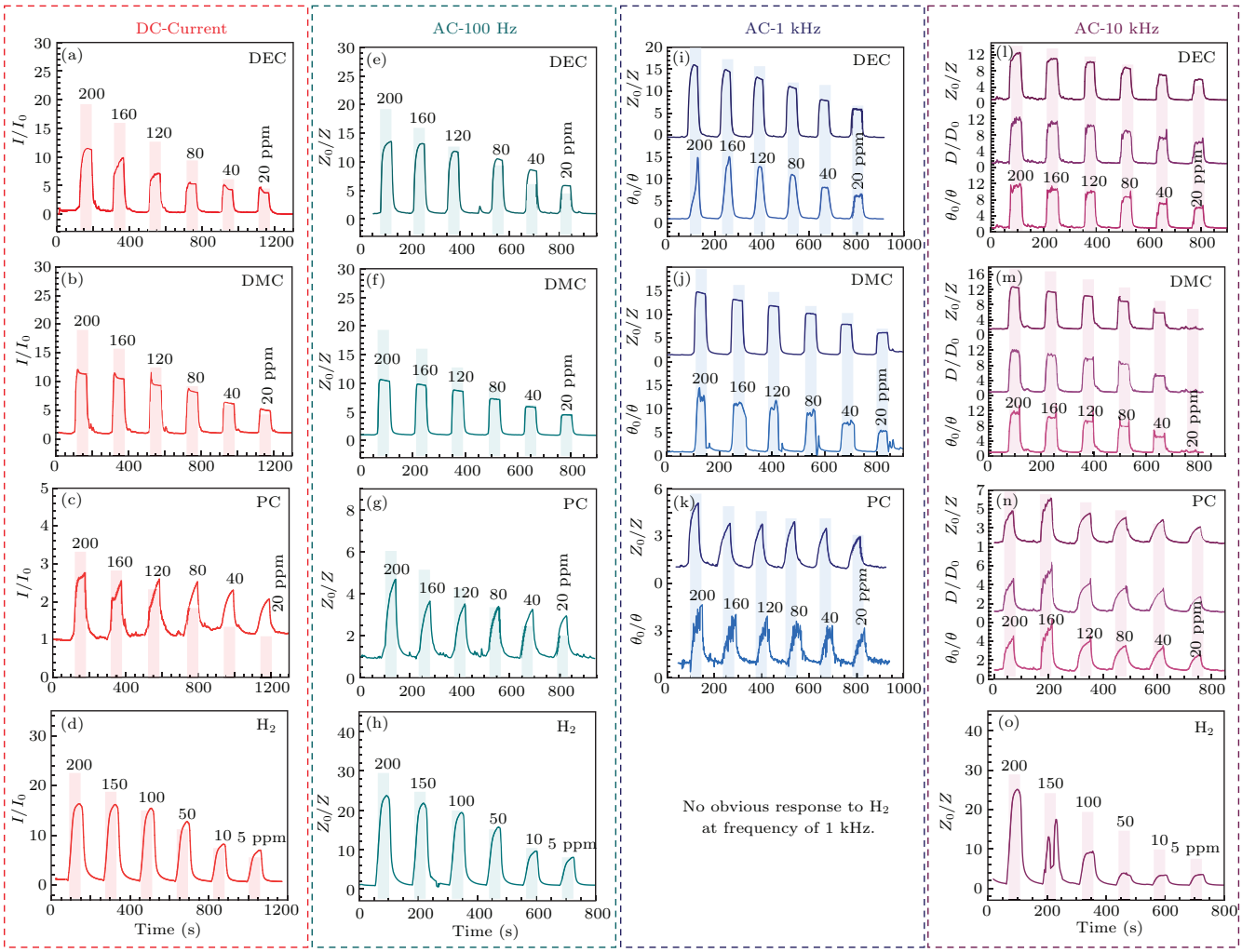


Fig. 2. Continuous response characteristics to different gases. DC current relative change (I/I_0) to a) DEC, (b) DMC, (c) PC and (d) H_2. AC impedance relative change (Z_0/Z) at the frequency of 100 Hz to (e) DEC, (f) DMC, (g) PC, and (h) H_2. AC impedance relative change (Z_0/Z) and θ relative change (θ_0/θ) at the frequency of 1 kHz to (i) DEC, (j) DMC, and (k) PC. AC impedance relative change (Z_0/Z), θ relative change (θ_0/θ), and D relative change (D/D_0) at the frequency of 10 kHz to l) DEC, (m) DMC, (n) PC, and (o) H_2. Here, I_0 (Z_0, θ_0 and D_0) and I (Z, θ and D) are the sensor DC current (AC impedance, phase angle, and dissipation factor) in ambient air and the real-time value in analyte gas, respectively.

Under DC mode, upon exposure to each analyte, the sensor current increases rapidly, and then decreases back to the original baseline when the analyte is off. DEC, DMC, PC and H_2 are all electron donors. Each of the analytes adsorbed on the n-type SnO_2 surface could contribute electrons to the conduction band of SnO_2, leading to an increase in the concentrations of the majority of electron carriers, consequently increasing the current of the SnO_2 device.

Under AC mode at the frequency of 100 Hz, only an impedance response could be detected for each analyte. Notably, at AC frequency of 1 kHz, both impedance and phase angle (θ) responses to DEC, DMC, and PC are obvious, but no responses to H_2. At AC frequency of 10 kHz, all the impedance, θ, and dissipation factor (D) responses to DEC, DMC, and PC are excellent, while only an impedance response to H_2 could be detected. Interestingly, the sensor impedance decreases quickly when exposed to each analyte, at different AC frequencies, and then quickly increases back to the original baseline when the analyte is off. Moreover, the phase angle has the same response and recovery trend, while the D has the opposite response and recovery trend to each analyte. A detailed explanation will be given in the following section.

Figure S2 shows that the gas response values increase as each analyte concentration increases. According to reported electrochemical gas sensors, the response could be empirically linearly expressed as[23]

$$\ln(\text{response}) = \ln a + b \ln C,$$

where C represents the analyte concentration, and a and b are constants, depending on the type of gas sensor and sensing material. Figure 3 displays linear plots of logarithms of the response value as a function of the logarithms of each analyte concentration under different modes, except for the impedance response to H_2 at 10 kHz. A similar linear relationship is seen in a previous report.[24] The relative parameters (slope, intercept, and R^2) of each fitting equation are summarized in Table 1.

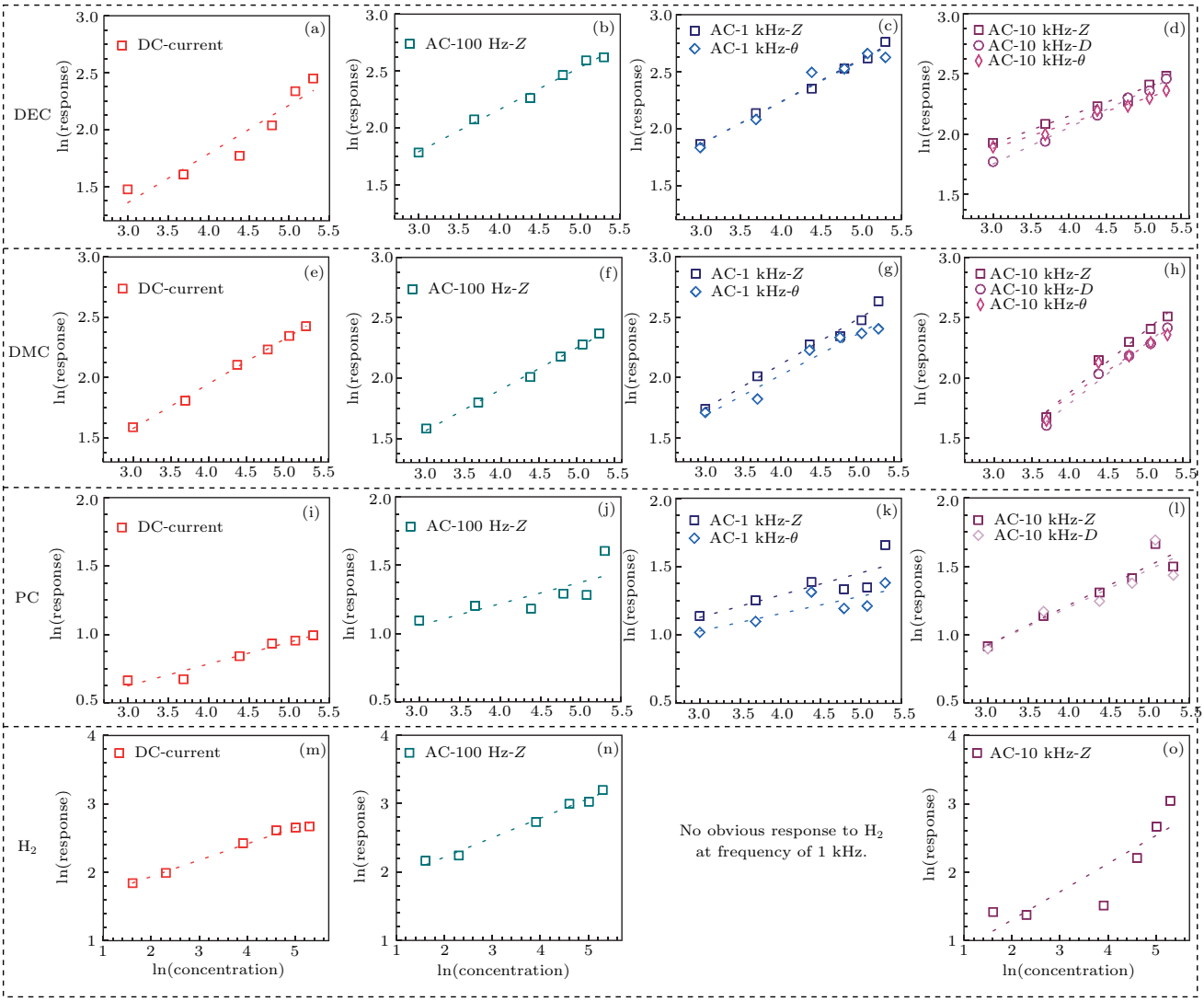


Fig. 3. The relationship of response values vs. concentration in logarithmic terms for different gases. DEC: (a) DC current, (b) AC impedance at the frequency of 100 Hz, (c) AC impedance and θ at the frequency of 1 kHz, (d) AC impedance, θ and D at the frequency of 10 kHz. DMC: (e) DC current, (f) AC impedance at the frequency of 100 Hz, (g) AC impedance and θ at the frequency of 1 kHz, (h) AC impedance, θ and D at the frequency of 10 kHz. PC: (i) DC current, (j) AC impedance at the frequency of 100 Hz, (k) AC impedance and θ at the frequency of 1 kHz, (l) AC impedance, θ and D at the frequency of 10 kHz. H_2: (m) DC current, (n) AC impedance at the frequency of 100 Hz, (o) AC impedance, θ and D at the frequency of 10 kHz. The symbols are response values; the lines are the fitting of response values vs. concentration.

Table 1. Slope, intercept, and R^2 values of the fitting equations of response vs. concentration for different gases under DC and AC dual modes.

Analyte gas	Parameters	DC-current	AC-100 Hz	AC-1 kHz		AC-10 kHz		
				Z	θ	Z	D	θ
DEC	slope	0.42731	0.36962	0.37532	0.37135	0.23043	0.29921	0.20401
	intercept	0.07851	0.68387	0.73479	0.7458	1.22798	0.85725	1.27225
	R^2	0.88011	0.99036	0.99335	0.94412	0.96935	0.99435	0.98272
DMC	slope	0.36817	0.3416	0.36531	0.33254	0.50813	0.48816	0.42507
	intercept	0.47468	0.54246	0.64702	0.68773	–0.15326	–0.16314	0.14677
	R^2	0.99756	0.99574	0.98367	0.94197	0.97114	0.98175	0.91323
PC	slope	0.15946	0.15725	0.16294	0.127	0.28948	0.27714	N.A.
	intercept	0.14599	0.58848	0.64014	0.6479	0.05747	0.09068	N.A.
	R^2	0.93059	0.52691	0.6176	0.63015	0.8975	0.78358	N.A.
H_2	Slope	0.2396	0.28512	N.A.	N.A.	0.41134	N.A.	N.A.
	intercept	1.45833	1.64665	N.A.	N.A.	0.47853	N.A.	N.A.
	R^2	0.9874	0.98291	N.A.	N.A.	0.70223	N.A.	N.A.

Moreover, a comparison of response values to different analytes (200 ppm DEC, DMC, PC, and H_2) under different modes is shown in Fig. 4. Obviously, for different signal modes, the selectivity of the sensor to the various analytes is different. The different selectivity enables various analyte recognition using one device.

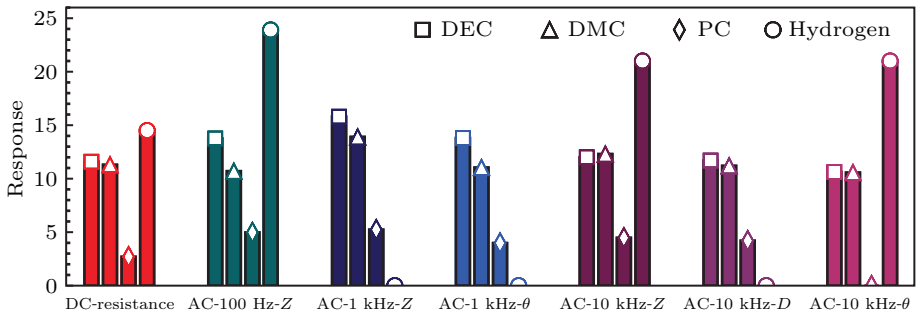


Fig. 4. A comparison of response values towards different gases under DC and AC modes (200 ppm DEC, DMC, PC and H_2).

In contrast to the operating principle of the DC current mode, the AC responses (including Z_0/Z, θ_0/θ, and D/D_0) are closely related to not only the conductivity of the sensing layer, but also the permittivity of the sensing material and analytes.[12] The equivalent circuit of the SnO_2 sensor with IDEs could be simply regarded as a typical Randles circuit, as depicted in Fig. 5. Here, R_1 and C_1 represent the time-constant resistance and capacitance of the SnO_2 layer, respectively. The parallel circuit element ($R_2 \parallel C_2$) corresponds to the resistance and capacitance of gas-dependent interfaces, which dominate the AC responses of the device.[12,25] The Warburg impedance, ascribed as Z_w, is as a result of the gas diffusion process, and only observed in the low-frequency regime (< 10 kHz).[25–27] The imaginary and real parts of impedance can be described by

$$Z_{\text{imaginary}} = -\frac{\omega R_1^2 C_1}{1+\omega^2 R_1^2 C_1^2}\text{j} - \frac{\omega R_2^2 C_2}{1+\omega^2 R_2^2 C_2^2}\text{j}, \tag{1}$$

$$Z_{\text{real}} = R_0 + \frac{R_1}{1+\omega^2 R_1^2 C_1^2} + \frac{R_2}{1+\omega^2 R_2^2 C_2^2}, \tag{2}$$

where ω represents the AC frequency.[12,25] The tested impedance value is calculated as follows:

$$Z = \sqrt{Z_{\text{imaginary}}^2 + Z_{\text{real}}^2}. \tag{3}$$

According to the Mott–Schottky equation, the capacitance of SnO_2 can be calculated as[28]

$$\frac{1}{C^2} = \frac{2}{\varepsilon\varepsilon_0 e A^2 N_{\text{d}}}\left(E - E_{\text{FB}} - \frac{kT}{e}\right), \tag{4}$$

where ε is the relative permittivity (dielectric constant), ε_0 is the vacuum permittivity, e is the electron charge, N_{d} is the majority carrier concentration, E is the applied electrical potential, k is the Boltzmann constant, and T is the absolute temperature.

The phase angle (θ) can be calculated by the following equation:

$$\theta = \arctan\left(\frac{Z_{\text{imaginary}}}{Z_{\text{real}}}\right). \tag{5}$$

The dissipation factor D can be calculated by the following equation:

$$D = \frac{Z_{\text{real}}}{Z_{\text{imaginary}}}. \tag{6}$$

Upon exposure to the analytes of electron donors, under AC modes, electrons will contribute to the SnO_2 surface due to analyte adsorption, and will result in a decrease in the gas-dependent interface resistance R_2. Beyond this, changes in the dielectric properties of analyte-dependent interfaces in a fixed frequency could also contribute to the impedance responses, according to Eqs. (1)–(4). The permittivities of DEC, DMC, PC and H_2 are 2.805, 3.107, 64.92 and 1, respectively.[29] Based on reports, the gas-dependent interface capacitance C_2 mainly relies on the dielectric constants of analytes.[25,30] Hence, C_2 has no significant effect on the AC responses of SnO_2 to DEC and DMC, due to their low permittivities. But for PC with high permittivity, C_2 generates an obvious AC response improvement, except for the θ response at 10 kHz.

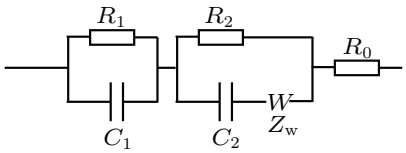


Fig. 5. The AC equivalent circuit of the SnO_2 sensor. R_0 represents phase constant contact resistance. The parallel circuit element ($R_1 \parallel C_1$) represents capacitance and resistance of the SnO_2 sensing layer. The parallel element ($R_2 \parallel C_2$) is the equivalent resistance and capacitance of the analyte-gas-dependent interface. The Warburg impedance is described as the Z_w.

Furthermore, the only detected Z response to each analyte at 100 Hz indicates that electronic resistance properties of gas-dependent interfaces mainly controls the sensing response. When the frequency increased to 1 kHz, an obvious capacitance effect appears, resulting in the detected Z and θ response; when the frequency further increased to 10 kHz, an additional D response could be detected with more capacitance effect (Figs. 2–3).

Interestingly, the impedance response of H_2 at 100 Hz was increased dramatically compared to the DC current response, although the permittivity of H_2 is also small. According to previous reports, it is proposed that the chemical species induced by H_2 adsorption enhances the AC impedance response at the low frequency of 100 Hz, via generation of a polarization potential in the H_2–SnO_2 interface.[12,31,32] When

the AC frequency increases to 1 kHz, no AC impedance-related parameter responses to H_2 could be detected. A similar sharp response decrement with the frequency increasing has previously been reported.[31,32] When the AC frequency further increases to 10 kHz, quick diffusion of H_2 plays an important role, with more capacitor effects (Z_w) due to the small molecular size, resulting in a non-linear impedance response to concentration.

3.3. Principal component analysis

PCA is a commonly used effective method in exploratory data analysis and classification. In the present work, differences in the various parameter responses to each analyte provide the possibility of multi-gas recognition based on one device. Utilizing Python and the PCA function in the Sklearn Library, the database was projected into a 2D plane. Visualization in a two-dimensional graph in Fig. 6 reveals that the electrolyte vapors and H_2 are actually and clearly discriminated. The mathematic derivation in the PCA code is attached in the supporting information. The cumulative variance of the principal components of over 97% (PC1 90.48% and PC2 6.52%) indicates that the major information is maintained from the raw database.

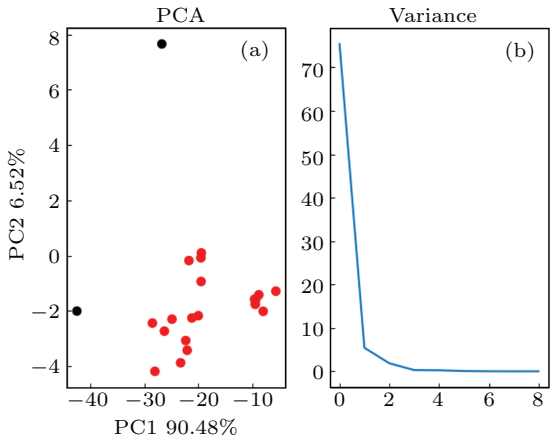


Fig. 6. (a) PCA-assisted classification and regression of electrolyte vapors (red dots) and H_2 (black dots). (b) Nine characteristic values of the covariance matrix for PCA.

4. Conclusions

In summary, smart and clear classification of electrolyte vapors and H_2 has been realized using a single common SnO_2 sensor, by combining DC current signals and AC impedance-related signals. Due to the dielectric properties of analytes, the SnO_2 sensing layer, and the analyte adsorption on the SnO_2 surface, diverse sensing parameters were obtained under DC and AC dual test modes, which enable the single sensor to build signature-difference patterns for tested gases via PCA analysis. The accurate distinction of electrolyte vapors and H_2 would contribute to the monitoring of the operating conditions of LIBs. This robust method for the classification and recognition of various chemical vapors using an individual device paves the way toward applications in intelligent identification of multi-gas with very few sensors.

Acknowledgements

This research was supported by the Zhejiang Science and Technology Foundation (Grant No. LQ20F040006).

The authors acknowledge L. M. for help with the SEM and XRD characterizations. Yan W. J. acknowledges the 2011 Zhejiang Regional Collaborative Innovation Center for Smart City.

References

[1] Jin Y, Zheng Z K, Wei D H, Jiang X, Lu H F, Sun L, Tao F B, Guo D L, Liu Y, Gao J F and Cui Y 2020 *Joule* **4** 1714
[2] Zhu X X, Jiang W, Wan Z W, Zhao S, Li Z H, Wang L G, Ni W B, Ling M and Liang C D 2021 *Energy Storage Science and Technology* **10** 848
[3] Liu K, Liu Y Y, Lin D C, Pei A and Cui Y 2018 *Sci. Adv.* **4** eaas9820
[4] Lu Y, Zhang S Q, Dai S L, Liu D P, Wang X, Tang W, Guo X J, Duan J, Luo W, Yang B B, Zou J, Huang Y H, Katz H E and Huang J 2020 *Matter-Us* **3** 904
[5] Du X W, Yang B, Lu Y, Guo X J, Zu G Q and Huang J 2021 *J. Mater. Chem. C* **9** 6760
[6] Kaur P, Bagchi S, Gribble D, Pol V G and Bhondekar A P 2022 *ACS Sens.* **7** 674
[7] Liao Z H, Zhang S, Li K, Zhang G Q and Habetler T G 2019 *J. Power Sources* **436** 226879
[8] Xu K 2004 *Chem. Rev.* **104** 4303
[9] Degler D, Weimar U and Barsan N 2019 *ACS Sens.* **4** 2228
[10] Walker J M, Akbar S A and Morris P A 2019 *Sensor Actuat. B-Chem.* **286** 624
[11] Lee J, Jung Y, Sung S H, Lee G, Kim J, Seong J, Shim Y S, Jun S C and Jeon S 2021 *J. Mater. Chem. A* **9** 1159
[12] Zhang B, Sun J Y and Gao P X 2020 *Adv. Mater. Technol.-Us* **5** 1901152
[13] Chen Y, Zhang H, Feng Z H, Zhang H X, Zhang R, Yu Y Y, Tao J, Zhao H Y, Guo W L, Pang W, Duan X X, Liu J and Zhang D H 2016 *Acs Appl. Mater. Inter.* **8** 21742
[14] Potyrailo R A 2016 *Chem. Rev.* **116** 11877
[15] Potyrailo R A 2017 *Chem. Soc. Rev.* **46** 5311
[16] Balasubramani V, Chandraleka S, Rao T S, Sasikumar R, Kuppusamy M R and Sridhar T M 2020 *J. Electrochem. Soc.* **167** 037572
[17] Moseley P T 2017 *Meas. Sci. Technol.* **28** 082001
[18] Bindra P and Hazra A 2020 *IEEE T. Instrum. Meas.* **69** 6621
[19] Sun H, Liu B S, Liu X and Yin Z D 2017 *J. Mater. Res.* **32** 2414
[20] Chen Y L, Li M J, Yan W J, Zhuang X, Ng K W and Cheng X 2021 *ACS Omega* **6** 1216
[21] Yan W J, Chen Y L, Zeng X M, Wu G, Jiang W, Wei D, Ling M, Ng K W and Qin Y X 2021 *Appl. Surf. Sci.* **535** 147697
[22] Yan W J, Xu H S, Ling M, Zhou S Y, Qiu T, Deng Y J, Zhao Z D and Zhang E P 2021 *ACS Sens.* **6** 2613
[23] Ma L T, Fan H Q, Tian H L, Fang J W and Qian X Z 2016 *Sensor Actuat. B-Chem.* **222** 508
[24] Mhlongo G H, Motaung D E, Cummings F R, Swart H C and Ray S S 2019 *Sci. Rep.* **9** 1
[25] Liu Y X and Lei Y 2013 *Sensor Actuat. B-Chem.* **188** 1141
[26] Stranzenbach M and Saruhan B 2009 *Sensor Actuat. B-Chem.* **137** 154
[27] Hagen G, Dubbe A, Rettig F, Jerger A, Birkhofer T, Muller R, Plog C and Moos R 2006 *Sensor Actuat. B-Chem.* **119** 441
[28] Adan-Mas A, Silva T M, Guerlou-Demourgues L and Montemor M F 2018 *Electrochim. Acta.* **289** 47
[29] Xu K 2004 *Chem. Rev.* **104** 4303
[30] Hendriks M G H M, ten Elshof J E, Bouwmeester H J and Verweij H 2002 *Solid State Ionics* **146** 211
[31] Deng Jie, Tan O K, Zhu W G, Chen X F and Yao X 2004 *IEEE T. Ultrason. FERR* **51** 923
[32] Kashif M, Ali M E, Ali S M U, Hashim U and Abd Hamid S B 2013 *Nanoscale Res. Lett.* **8** 1